

Local and remote temperature response of regional SO₂ emissions

Anna Lewinschal^{1,2}, Annica M. L. Ekman^{1,2}, Hans-Christen Hansson^{2,3}, Maria Sand⁴, Terje K. Berntsen^{4,5}, and Joakim Langner⁶

¹Department of Meteorology, Stockholm University, Stockholm, Sweden

²The Bolin Centre for climate research, Stockholm University, Stockholm, Sweden

³Department of Environmental Science and Analytical Chemistry, Stockholm University, Stockholm, Sweden

⁴CICERO Center for International Climate and Environmental Research, Oslo, Norway

⁵University of Oslo, Department of Geosciences, Oslo, Norway

⁶Swedish Meteorological and Hydrological Institute, Air Quality Research Unit, Norrköping, Sweden

Correspondence: Anna Lewinschal (anna@misu.su.se)

1 **Abstract.** Short-lived anthropogenic climate forcers, such as sulphate aerosols, affect both climate and air quality. Despite
2 being short-lived, these forcers do not affect temperatures only locally; regions far away from the emission sources are also
3 affected. Climate metrics are often used e.g. in a policy context to compare the climate impact of different anthropogenic
4 forcing agents. These metrics typically relate a forcing change in a certain region with a temperature change in another region
5 and thus often require a separate model to convert emission changes to radiative forcing changes.

6 In this study, we used a coupled Earth System Model (NorESM) to calculate emission-to-temperature-response metrics for
7 sulphur dioxide (SO₂) emission changes in four different policy-relevant regions: Europe, North America, East Asia and South
8 Asia. We first increased the SO₂ emissions in each individual region by an amount giving approximately the same global
9 average radiative forcing change (-0.45 Wm⁻²). The global mean temperature change per unit sulphur emission compared to
10 the control experiment was independent of emission region and equal to $\sim 0.006\text{K/TgSyr}^{-1}$. On a regional scale, the Arctic
11 showed the largest temperature response in all experiments. The second largest temperature change occurred in the region of
12 the imposed emission increase, except when South Asian emissions were changed; in this experiment, the temperature response
13 was approximately the same in South Asia and East Asia. We also examined the non-linearity of the temperature response by
14 removing all anthropogenic SO₂ emissions over Europe in one experiment. In this case, the temperature response (both global
15 and regional) was twice of that in the corresponding experiment with a European emission increase. This nonlinearity in the
16 temperature response is one of many uncertainties associated with the use of simplified climate metrics.

17 *Copyright statement.* TEXT

18 1 Introduction

19 Anthropogenic emissions of short-lived climate forcers (SLCFs), i.e. chemical components in the atmosphere that interact
20 with radiation, have both an immediate effect on local air quality and regional and global effects on the climate in terms of

21 e.g. changes in the temperature and precipitation distribution. Aerosol particles are one of the most important SLCFs due to
22 their abundance and their effects on health and climate. The short atmospheric residence times of SLCFs such as sulphate
23 and carbonaceous aerosols (around days) lead to high atmospheric concentrations in emission regions and a highly variable
24 radiative forcing pattern. Regional radiative forcing can, nevertheless, exert a large influence on the temperature field away
25 from the forcing region through changes in heat transport or the atmospheric or ocean circulation (Menon et al., 2002; Shindell
26 et al., 2010; Lewinschal et al., 2013; Acosta Navarro et al., 2016; Dong et al., 2016). Here, we investigate the effect of sulphate
27 aerosol precursor emission perturbations in different regions on the global surface temperature distribution using a global
28 climate model.

29 The local radiative forcing by a unit aerosol emission varies from region to region depending on a number of factors,
30 including e.g. emission location, aerosol processing in the atmosphere and removal rates as well as land surface properties and
31 cloud distribution (e.g. Bellouin et al., 2016). Moreover, a unit radiative forcing in a specific region may have different impacts
32 on the temperature response locally in the forcing region and in remote regions away from the forcing, as well as between
33 different remote regions. In other words, the climate sensitivity in one region can vary depending on the location of the forcing
34 (e.g. Shindell and Faluvegi, 2009).

35 To facilitate comparisons of the climate effect of different greenhouse gases and emission levels, several climate metrics
36 have been developed which connect emission changes to radiative forcing, or a specified forcing to a temperature response
37 (e.g. Aamaas et al., 2013). One appeal of simple climate metrics is that they provide a way to easily evaluate the climate impact
38 of different air quality or climate mitigation policies without having to run a coupled climate model, something which is not
39 always feasible due to the computational costs. Because of the even spatial distribution of long lived greenhouse gases, these
40 metrics have usually described global average quantities. However, the highly variable spatial distribution of aerosol forcing
41 necessitates the use of metrics that take these spatial inhomogeneities into account (Shine et al., 2005).

42 Shindell and Faluvegi (2009) developed a metric that accounts for spatial inhomogeneities both in the forcing and tempera-
43 ture response, the Regional Temperature Potential (RTP). With a large set of simulations with one climate model, where they
44 varied the location of forcing from various anthropogenic climate forcers, these authors derived RTP coefficients that link the
45 radiative forcing from a climate forcer in a specific region to regional temperature responses. An evaluation of the method for
46 transient simulations of historical aerosol forcing and response with four different climate models was presented in the work
47 of Shindell (2012).

48 However, the simplification inherent in the climate metric concept might lead to difficulties related to the generality of these
49 metrics, such as the RTP. Differences between RTP coefficients derived from different climate models can stem from a number
50 of different sources, involving everything from atmospheric processing of aerosols, interaction with radiation, aerosol cloud
51 effects or climate feedbacks, and how these processes are represented in different climate models (Kasoar et al., 2016; Conley
52 et al., 2018).

53 The main objective of this study is to investigate the global and remote impacts of regional sulphate aerosol precursor
54 emission changes on the surface temperature distribution. This is done by using a coupled atmosphere-ocean model with
55 interactive aerosol representation, the Norwegian Earth System Model (NorESM). The results from the model simulations are

56 used to derive RTP coefficients similar to the work of Shindell and Faluvegi (2009). However, our method for deriving RTP
57 coefficients differs from that of Shindell and Faluvegi (2009) in that we derive our RTP coefficients directly from emission
58 perturbations and focus primarily on the emissions-temperature connection rather than the connection between radiative forcing
59 and temperature, similar to Kasoar et al. (2018). The RTP coefficients derived by Shindell and Faluvegi (2009) describe the
60 regional temperature change in response to regional radiative forcing, and essentially describe a regional sensitivity. These
61 forcing-based sensitivities have to be combined with the radiative forcing patterns derived from emission scenarios with a
62 chemistry transport model or offline calculations for radiative forcing with a general circulation model to provide the emission-
63 temperature connection. Another difference is that we focus on emissions from air-pollution and policy-making relevant regions
64 rather than the latitudinal bands of Shindell and Faluvegi (2009). Thus, we seek to investigate how much an emission change
65 in one policy relevant region affects both local climate as well as the climate on global scale and in remote regions.

66 The aim is that the RTP coefficients derived with NorESM eventually could be used in Integrated Assessment analysis (IAA),
67 e.g. such as the Greenhouse gas - Air pollution Interactions and Synergies (GAINS) model. In the GAINS model the climate
68 impact is estimated using the Global Warming Potential (GWP), which is the global radiative forcing integrated over time
69 normalised by that of CO₂ (Amann et al., 2011). By the GWP the global climate impact of SLCFs can be taken into account.
70 Lately, the radiative forcing of long-lived greenhouse gases other than CO₂ have been included in GAINS, which makes it
71 possible to evaluate the changes emissions of these due to air pollution abatement. Using RTP coefficients in IAA would mean
72 that not only near-term climate effects of changed SLCF emissions can be evaluated but also how different regions are affected
73 due to specific regional abatement measures. The RTP can be based on different entities as radiative forcing, effective radiative
74 forcing or direct emissions, which need very different support calculations respectively. Using the emissions as base for RTPs
75 will provide a very simple way to estimate the climate impact of changed emissions without having to run a chemical transport
76 model. Using any of the bases for the RTPs avoids running large coupled climate models. However, the validity of this method
77 relies on the accuracy of the assumption that the temperature response to changed emissions is linear and that the interaction
78 between different SLCF are negligible for the resulting temperature response. To address the question regarding linearity in
79 the response depending on emission perturbation strength we perform simulations with different emission perturbations for the
80 European region.

81 The layout of this study is as follows. First an introduction to the RTP methodology is presented in the method section. The
82 NorESM model is described together with the experimental design to derive the emission specific RTP coefficients. In Sect.
83 3 we first present the results from experiments where sulphate aerosol precursor emissions were increased and the global and
84 regional effect of these emission perturbations. The results of an experiment where European anthropogenic sulphate aerosol
85 precursor emissions were removed are discussed in the context of non-linearities emerging as a consequence of emission
86 magnitudes. Last in the Result section is a comparison of the performance of the forcing-based RTP coefficients of Shindell and
87 Faluvegi (2009) and Shindell et al. (2012) for NorESM results. The Result section is followed by a discussion and conclusions.

89 **2.1 The Absolute Regional Temperature Potential**

90 There exists a number of different climate metrics that describe the connection between emissions of atmospheric tracer species
 91 and/or their radiative forcing and/or their effect on the global mean temperature. Many have been developed for the purpose
 92 of evaluating the impact of increased emissions of long-lived and well-mixed greenhouse gases. Thus, the connection between
 93 the location of an emission perturbation and the temperature response has not been a primary concern. However, for SLCFs
 94 the location of the emission perturbation and radiative forcing is a primary matter of interest. A climate metric which takes the
 95 spatial distribution of these SLCFs and the temperature response into account was developed by Shindell and Faluvegi (2009)
 96 and Shindell and Faluvegi (2010). The metric describes the temperature change dT in one area a at time t , in response to
 97 forcing F in area a' :

$$dT_a(t) = \int_0^t \left(\sum_{a'} F_{a'}(t') \cdot \frac{dT_a/F_{a'}}{dT_a/F_{global}} \right) \cdot IRF(t-t') dt', \quad (1)$$

98 where the numerator in the second term of the sum, $dT_a/F_{a'}$, is the regional response coefficient (cf. Table 3 of Shindell
 99 and Faluvegi (2010)), which, in this formulation is normalised by the regional temperature response to global average forcing,
 100 dT_a/F_{global} . The Impulse Response Function, IRF , represents the time dependent temperature response per unit forcing, i.e.
 101 the climate sensitivity. For the equilibrium (or quasi-equilibrium or transient) temperature response to a steady forcing, the
 102 IRF can be replaced by the equilibrium or transient climate sensitivity, λ .

103 Shindell (2012) elaborated the regional temperature change metric of Shindell and Faluvegi (2010) to an Absolute Regional
 104 Temperature potential, $ARTP$, which, in analogue to the Absolute Global Temperature change Potential (AGTP), connects an
 105 emission perturbation, E , in region r of a climate forcer to an absolute temperature change (Shine et al., 2005) in area a :

$$ARTP_{a,r}(t) = \int_0^t \left(\sum_{a'} \frac{F_{a'}(t')}{E_r} \cdot \frac{dT_a/F_{a'}}{dT_{global}(F_{global})/F_{global}} \right) \cdot IRF(t-t') dt'. \quad (2)$$

106 This formulation uses the global climate sensitivity ($dT_{global}(F_{global})/F_{global}$) to normalise the regional response coeffi-
 107 cients in contrast to Eq. 1 which uses the regional sensitivity to global forcing. This, i.e. the second term in the summation of
 108 Eq. 2, yields the unitless RTP coefficients presented in Table 1 of Shindell (2012). Shindell (2012) also advocate the use of the
 109 latter formulation (Eq. 2) before the former (Eq. 1).

110 The RTP coefficients provided in the work of Shindell and Faluvegi (2010) and Shindell (2012) were derived for forcing in
 111 four latitude bands covering the globe: the Southern Hemisphere extratropics (90-28°S, SHext), Tropics (28°S-28°N), Northern
 112 Hemisphere mid latitudes (28-60°N, NHml) and Arctic (60-90°N). These RTP coefficients can be used to estimate the global
 113 temperature response to any emission perturbation, as long as the forcing in response to the emission perturbation in each of

114 the latitude bands described above is known. The forcing distribution in response to an emission perturbation can be calculated
115 with e.g. a chemistry transport model (direct radiative forcing only), or with atmospheric general circulation models.

116 In this work, we take our starting point in emission perturbations rather than in the forcing distribution. Sub-global tem-
117 perature changes in response to emission perturbations are derived both for latitudinal bands following Shindell and Faluvegi
118 (2009) as well as for the emission regions defined in this study, with the addition of a complementary Arctic region (AR).
119 This complementary Arctic region is defined as the area north of the Arctic circle (66°N), whereas the northernmost latitudinal
120 band (hereafter denoted ARCT) is defined as the area north of 60°N in accordance with the definition of Shindell and Faluvegi
121 (2009). All regions that are used in this study are listed in Table 1.

122 **2.2 NorESM**

123 The regional temperature changes in response to aerosol emission perturbations are investigated using NorESM (Bentsen
124 et al., 2013). This model is based on the Community Climate System Model 4.0 (CCSM4.0), but has been modified to include
125 interactive aerosols and to use the Bergen version of the Miami Isopycnic Coordinate Ocean Model (MICOM) instead of the
126 Parallel Ocean Program (POP) model. For NorESM the atmospheric component of the model, the Community Atmospheric
127 Model version 4 (CAM4) has been extended with an interactive aerosol module, CAM4-Oslo (Kirkevåg et al., 2013). The land
128 surface is represented by the Community Land Model version 4 (CLM4) and sea-ice is modelled with the ice model CICE4.
129 The atmospheric model uses a finite volume grid with a resolution of $1.9^{\circ}\times 2.5^{\circ}$ latitude-longitude.

130 The aerosol module in NorESM considers five different aerosol components: sulphate, black carbon, organic matter, mineral
131 dust and sea salt. Both the mass and number for these aerosol constituents are predicted in a combined sectional and modal
132 framework. Emissions take place both in the form of primary particles and as precursors to aerosols where the aerosol chemical
133 compounds are produced through aqueous and gas phase chemical reactions. Aerosols can exist both as external and internal
134 mixtures, depending on atmospheric processing. For example, sulphate coating of black carbon, which changes the optical
135 and hygroscopic properties of this internally mixed aerosol compared with the externally mixed constituents, is accounted for.
136 Humidification of aerosols is based on the hygroscopicity of the aerosol and the atmospheric relative humidity. Aerosols are
137 removed from the atmosphere by dry and wet deposition.

138 Aerosol can affect cloud properties through acting as cloud condensation nuclei (CCN). The efficiency of a particular aerosol
139 depends on its hygroscopicity and size. The amount of aerosol particles that are efficient CCN is connected to the predicted
140 aerosol size and mass and connected to the two-moment cloud microphysics for stratiform clouds in the model. Thus, NorESM
141 simulates both the cloud albedo effect and cloud lifetime effects of aerosols. Beside these effects of aerosols on cloud mi-
142 crophysical properties, semidirect effects which depend on changes of the thermal structure of the atmosphere are accounted
143 for.

144 An evaluation of the performance of NorESM in simulating the present climate was carried out by Bentsen et al. (2013),
145 who identified the main biases in the modelled climate compared to observations and that the model simulates a stable climate.
146 Iversen et al. (2013) derived climate sensitivities for NorESM and investigated the climate response to different future emission

147 scenarios. They found that the CO₂ climate sensitivity of the model is smaller than the Coupled Model Intercomparison Project
148 phase 5 (CMIP5) multi-model mean, but within one standard deviation.

149 **2.3 Experiments**

150 We perform a suite of model simulations with NorESM where aerosol precursor emissions are perturbed in one region at a
151 time. Four regions which we consider being of particular interest from an aerosol and air-pollution perspective are studied:
152 Europe, North America, South Asia and East Asia. The emissions of anthropogenic aerosols have changed considerably in
153 these regions during the 20th century (e.g. Lamarque et al., 2010).

154 The emission regions (North America - NA, Europe - EU, South Asia - SA and East Asia - EA) are defined according
155 to the updated region definition of the Task Force on Hemispheric Transport of Air Pollution (HTAP), see Fig. 1, and the
156 aerosol emissions are the historical emissions of CMIP5 described by Lamarque et al. (2010). The aerosol type we study here
157 is ammonium sulphates and thus we perturb the anthropogenic sulphur dioxide (SO₂) emissions provided for CMIP5.

158 Year 2000 is chosen as the baseline year and aerosol emissions, aerosol precursor emissions, trace gas concentrations and
159 land use representing this year are used for the control simulation. In the emission perturbation experiments, the anthropogenic
160 aerosol precursor emissions are decreased or increased compared to year 2000 emissions and kept constant in each region
161 throughout the simulation. In total five coupled sensitivity experiments were performed, four experiments where SO₂ emissions
162 were increased in the four different regions and one where anthropogenic SO₂ emissions were removed over Europe. The
163 simulations were started from year 2000 in the transient historical CMIP5 simulation. The simulation length is 160 years
164 for simulations where emissions are increased. For the experiment where emissions are decreased the simulation length is
165 200 years. All the results presented are annual mean quantities and the first 50 years of each simulations have been removed
166 before averaging and are tested for statistical significance with a student's t-test. Uncertainty ranges for the results are given as
167 standard errors or standard deviations derived from the variability in each simulation.

168 The SO₂ emission changes in the emission perturbation experiments are shown in Fig. 2. In the 0xEU experiment the SO₂
169 emissions in Europe are not completely eliminated. There remains 4.66 Tgyr⁻¹ of volcanic emissions of SO₂ in Europe (from
170 Etna). The SO₂ emissions in the rest of the experiments were increased by varying amounts depending on the magnitude of
171 the regional emissions in the control simulation. This was done to obtain a global mean instantaneous radiative forcing of
172 approximately -0.45 Wm⁻² in all these perturbation experiments. For South Asian emissions, which are low in the control
173 simulation (6.47 Tgyr⁻¹ in year 2000 compared with 24.53 Tgyr⁻¹ in East Asia) the emissions were increased by a factor
174 of ten. Similarly, for Europe, North America and East Asia, SO₂ emissions were increased by a factor of seven, five and five
175 respectively.

176 The 0xEU experiment is included so that the effect of emission perturbation magnitude can be investigated, i.e. the sensitivity
177 to a relatively small emission reduction compared to a relatively large emission increase. The emission perturbation magnitude
178 (and sign, i.e. reduction) could also be considered as a more likely future scenario.

179 With the resulting global temperature response field of each emission perturbation experiment, RTP coefficients, dT_a/dEm_r ,
180 can be constructed relating emission changes in the predefined emission regions, r , to any response region, a , of choice. The
181 emission-based ARTP can be calculated from the absolute emission change:

$$ARTP_{a,r}^{EM} = \Delta Em_r \frac{dT_a}{dEm_r}. \quad (3)$$

182 In addition to the coupled experiments we perform simulations to evaluate the Instantaneous Radiative Forcing (RF) and
183 Effective Radiative Forcing (ERF) of the aerosol emission perturbations in the coupled experiments.

184 The RF is derived from fixed Sea Surface Temperatures (SSTs) simulations where dual calls are made to the radiation
185 code: one call with the CAM4 climatological aerosols and another call where the emission perturbation aerosol concentrations
186 and their effect on cloud albedo are sent to the radiation code solely for diagnosing the radiative effect of these. Thus the
187 meteorology in the RF simulations is identical since the radiative effects of the emission perturbations do not feedback on the
188 meteorology. Similarly, a dual call control simulation with year 2000 aerosol emissions was performed. With this methodology
189 the radiative effects alone from the aerosol can be quantified, without influence of fast or slow feedbacks. The RF simulations
190 are 7 years long and the 5 last years are used for the analysis.

191 The ERF is derived by performing fixed SST simulations with aerosol emission perturbations and letting the radiation
192 changes affect the meteorology. These simulations are compared to a fixed SST simulation with year 2000 aerosol emissions.
193 Thus, in addition to the aerosol direct radiative effect and cloud albedo effect the ERF also includes radiative changes from
194 fast feedbacks such as cloud microphysical and semidirect effects. In NorESM these effects includes e.g. cloud liquid water
195 content and cloud fraction. These simulations are 20 years and the 15 last years are used for the analysis. Similarly to the
196 coupled simulations, the RF and ERF are tested for statistical significance with the student's t-test. Standard errors and standard
197 deviations from the simulations are used to indicate the uncertainty range.

198 In a simplified manner, the process chain from emission to global mean temperature response can be thought of a translation
199 of emission to column burden, to the instantaneous direct and indirect radiative forcing, to forcing including fast feedbacks, to
200 the full coupled temperature response. In an attempt to identify where the largest divergence appears in the process chain from
201 emission to temperature response in the experiments conducted with NorESM, we investigate the usefulness and accuracy of
202 alternative quantities to the unit emission in predicting the surface temperature response.

203 **3 Results**

204 **3.1 Global forcing and temperature response**

205 The simplest way to describe the sulphur emission perturbation impact on global and regional temperatures is to express
206 the temperature response in terms of temperature change per unit emission of sulphur (cf. Sect. 2.1). We first analyse the
207 results from the sensitivity experiments where SO₂ emissions were increased. The results from the 0xEU experiment will be
208 discussed in Sect. 3.3. The global mean temperature response per unit emission for these sensitivity experiments where the

209 SO₂ emissions were increased by comparable magnitudes, the global temperature change per unit emission is similar within
210 10%. The temperature response varies from -0.0056 to -0.0061 K(TgSyr⁻¹)⁻¹, depending on the location and magnitude of
211 the sulphur emission change (Table 2).

212 All global mean temperature changes are significantly different compared to the temperature of the year 2000 control sim-
213 ulation, but are not significantly different between each other (Fig. S1a in supplementary material). Thus, the location of an
214 emission change does not appear to be a governing factor for the global mean temperature response modelled by NorESM.
215 However, all emission changes are located in the northern hemisphere, and atmospheric transport of aerosol particles will con-
216 tribute to a redistribution of atmospheric concentrations and the resulting column burden and radiative forcing of the aerosol,
217 so that in some cases the resulting column burden and radiative forcing from emission changes in different regions will partly
218 overlap.

219 The global average RF per unit emission change (Table 2) shows larger variability than the global temperature response
220 (varying from -0.010 to -0.017 Wm⁻²(TgSyr⁻¹)⁻¹, the largest RF value being 62% larger than the smallest value), a larger
221 emission change is needed in EU than in SA to obtain the same RF change. The variability for the global mean ERF is similar
222 to that of the RF (difference of 64% between the largest and smallest value, varying from -0.008 to -0.026 Wm⁻²(TgSyr⁻¹)⁻¹)
223 but the magnitude of the global mean ERF is smaller than the RF for all emission-increase experiments except for the 5xNA
224 experiment. Thus, on a global scale, fast cloud feedbacks contribute to dampen the forcing effect of the emission increases in
225 the NorESM experiments presented here.

226 3.1.1 Emission changes as predictor of global mean temperature change

227 As outlined in Sect. 2, the extreme simplification inherent in the method of describing the temperature response in terms of
228 emission perturbations, leads to uncertainties related to the generality of the RTP coefficients.

229 Figure 3a illustrates how SO₂ emission perturbations in the different experiments translate to global sulphate column burden,
230 RF, ERF and temperature anomalies. All values are normalised by the response in the North American experiments to illustrate
231 the relative amount of variability for each response quantity (i.e. response in the 5xNA experiment is always one in Figure 3.)

232 As noted previously, the global temperature responses per unit emission in the experiments where SO₂ emissions are in-
233 creased are not significantly different from each other. However, the translation from emission to column burden shows a
234 different pattern. For this quantity, the column burden per unit emission in the 10xSA experiment is 76% higher than in the
235 other experiments. Thus, the geographical location seems to be one factor controlling the column burden sensitivity to emis-
236 sion perturbations in the experiments where emissions are increased. The increased emissions in SA together with a local SA
237 reduction in precipitation of 0.22 mmday⁻¹ lead to a longer residence time of sulphate (0.73 days longer) as well as other
238 aerosol particles in NorESM in the 10xSA experiment compared to the control experiment.

239 A similar pattern as the column burden is evident for the normalised instantaneous RF response to a unit emission change.
240 The RF response to a unit emission change in SA is larger than the responses in the other experiments. Thus, there appears to
241 be a close connection between changes in the global sulphate column burden and the RF. The normalised ERF sensitivity to
242 unit emission perturbations, shows a larger variability between the experiments compared to the other investigated quantities.

243 The standard deviations for the global average ERF responses are also larger than that for RF. This result indicates that cloud
244 feedbacks, such as changes in liquid water content or cloud fraction and cloud albedo contribute substantially to the ERF (cf.
245 Table S1 in supplementary material), and also contributes to larger variability.

246 Figure 3b shows the temperature response normalised by the different "basis quantities" (i.e. the leftmost group of bars in
247 Fig. 3b are identical to the rightmost bars in Fig. 3a). The perfect basis quantity would be one for which the heights of all
248 bars corresponding to the different experiments are equal. A basis quantity with this property would be the ideal predictor
249 of the global mean temperature response. Figure 3b shows that emission perturbation is a good predictor of the temperature
250 response for emission increases from all regions investigated when emissions are increased in all regions (standard deviations
251 corresponding the each group of bars are presented in Table 3). Instantaneous RF and column burden as basis quantities
252 underestimate the temperature response to SA emissions (this is connected to the larger column burden and RF sensitivity
253 to a unit emission perturbation in SA which do not translate to a larger temperature sensitivity). For ERF there is substantial
254 variability in the predictability for the temperature responses in the emission increase experiments, which also yields the largest
255 standard deviation of the basis quantities for these experiments.

256 3.2 Sub-global forcing and temperature response

257 3.2.1 Latitudinal forcing and temperature response

258 The sub-global normalised temperature responses in the experiments where SO₂ emissions were increased display more varia-
259 tion between the different experiments than the global mean sensitivities. (As mentioned before, the 0xEU experiment will be
260 discussed in Sect. 3.3.2.) The latitudinal temperature responses per unit emission in the experiments with increased emissions
261 show a qualitatively similar pattern of increasing sensitivity with increasing latitude (Fig. 4). This pattern of Arctic amplifi-
262 cation is not dependent on the location of the emission perturbation in these experiments, neither in the latitudinal nor the
263 longitudinal direction. The temperature responses in each latitude band are significantly different from the temperature in the
264 year 2000 control simulation (at the 99% confidence level), except for the southern hemisphere temperature responses (indi-
265 cated by gray shading of the columns in Fig. 4). The latitudinal temperature responses in the different experiments are not
266 significantly different from each other, with the exception of most of the latitudinal temperature responses to SA emissions (at
267 the 90% confidence level, see Fig. S1 for details). Thus, the latitudinal temperature responses are in principle indistinguishable
268 for emission increases from EU, NA and EA, while the SA emission response is weaker in NHml and ARCT while it is stronger
269 in SHext and Tropics compared to the other experiments. The spatial distributions of the temperature responses are shown in
270 Figure 5.

271 The only latitudinal RF and ERF that are statistically significant are the responses to emissions increases in EU, NA and
272 EA, in NHml, the latitudinal band inside which these emission regions are located (Fig. 6). Significant ERF responses are also
273 found in ARCT for the same emission source regions, but the ERF is larger in NHml where the emissions changes are located,
274 than in ARCT. SO₂ emissions increases in SA do not lead to any latitudinal average RF or ERF response that are statistically
275 significant. A large fraction of the atmospheric sulphur mass from SA emissions (which are mainly emitted in the Tropics)

276 is transported to the NHml region, so that the average RF, ERF and column burden in this region exceeds that of the tropical
277 region. However, the total integrated sulphur column burden is larger in the Tropics than in the NHml (not shown) in the 10xSA
278 experiment.

279 The ERF acts to enhance the forcing relative to the RF in the NHml in all experiments, as well as in the ARCT region.
280 This is a manifestation of aerosol indirect effects which lead to e.g. higher cloud water content (Table S1). The ERF displays
281 a warming effect in the SHext (see also Figure 7) in all experiments (due to decreases in low cloud fraction at southern
282 hemisphere midlatitudes, not shown), although this positive ERF is not significant in any experiment. However, the positive
283 ERF in the southern hemisphere, which represents a large part of the global mean, contributes to the lower value of global
284 average of the ERF compared to the RF (cf. Sect. 3.1).

285 As described above, the temperature responses in the latitudinal bands are similar between the experiments with the excep-
286 tion of the temperature responses to changed SO₂ emissions in SA. SA has the largest tropical response which, however, is only
287 significantly different from the tropical response to EU emissions, which is the weakest tropical response among the experi-
288 ments. Similarly, the ARCT response to SA emissions is the smallest among the experiments, and is only significantly different
289 to the ARCT response to NA emissions, which leads to the strongest response in ARCT. The weaker NHml response to SA
290 emissions compared to the other emission regions, on the other hand, is significantly different compared to all other NHml
291 temperature responses. The NA, EU and EA emission regions are to the greater part located in the northern hemisphere mid-
292 latitudes, and mostly north of the SA emission region. Thus, the longitudinal position of a mid-latitude emission perturbation
293 does not appear to matter for the latitude mean temperature responses at northern hemisphere high- and mid-latitudes.

294 3.2.2 Regional temperature response

295 The differences between the sub-global temperature responses in the different experiments become more evident when they
296 are derived for the emission perturbation regions (and the AR region north of 66°N) compared to when derived for latitudinal
297 bands (Fig. 8). All regional temperature changes are statistically significant compared to the control simulation. The largest
298 temperature response is found in the AR region in all experiments, which is consistent with the latitudinal distribution of
299 the temperature response for latitude bands described in the previous section. Similarly, the SA emissions have the smallest
300 effect on the AR temperature among the experiments, but the AR temperature response in this experiment is only significantly
301 different from the response to NA emissions, which give the largest AR response among the experiments.

302 Outside the AR region, the largest temperature response is found locally in the emission region in all experiments except
303 10xSA. This result is consistent with the forcing always being largest in the emission region (Fig. 9). The regional RF and ERF
304 is also statistically significant for local SO₂ emissions from SA, as opposed to when derived for the Tropical latitudinal band
305 (Fig. 6). For SA emissions the temperature response in the EA region is marginally larger than the local temperature response
306 in the SA region. The EA region is located downwind of the SA region, which means that a substantial part of the sulphur
307 emitted in SA is transported to EA and contribute to the local forcing in EA. The column burden increases by 3%/TgSyr⁻¹ in
308 EA due to SA emission, to be compared with the increase in EA due to local emission of 4%/TgSyr⁻¹. Additionally, advection
309 of air originating from SA might also partly explain the large temperature response in the EA region to SA emissions. EA is the

310 only region where there are emissions from a remote region (SA) that lead to a temperature response that is indistinguishable
311 from the effect of local emissions.

312 The local temperature responses in the emission perturbation regions are larger than the corresponding zonal mean temper-
313 ature responses of the latitudes covered by each region (indicated by black dots in Fig. 8) in all experiments. The largest local
314 response relative to the zonal mean is found in the 10xSA experiment, which is 66% larger than the zonal mean. The 5xNA
315 experiment shows the largest absolute difference between the local response and the zonal mean, $0.0055 \text{ K/TgSyr}^{-1}$ (55%
316 larger). The smallest local temperature response relative the zonal mean is found for 7xEU (20%). All differences between
317 these local responses and the corresponding zonal means are statistically significant at the 95% confidence level.

318 For both NA and EU emission perturbations, the temperature responses in the regions outside the emission regions are close
319 to the corresponding zonal mean responses (within 2-17% difference). SA and EA emission perturbations, on the other hand,
320 both lead to a larger temperature response than the corresponding zonal mean for NA and a smaller temperature response than
321 the zonal mean for EU, where both these differences between the zonal mean and regional temperature response are statistically
322 significant. Both EA and SA emission perturbations have a substantial effect on NA temperature, of the same magnitude as the
323 local responses for these emission regions, despite the geographical distance between the emission location and the temperature
324 response regions. Local radiative forcing in NA is not responsible for this temperature effect (Fig. 9). This result points towards
325 a far field effect in the temperature response to Asian aerosol forcing which is mediated by atmospheric circulation changes
326 rather than radiation changes.

327 **3.3 Nonlinearities**

328 So far, only the results from the experiments where SO_2 emissions were increased have been discussed. In this section we will
329 focus on the differences between the results from the 0xEU and 7xEU SO_2 emission changes experiments. The purpose is to
330 investigate if the emission perturbation magnitude or background state influences the temperature response (cf. e.g. Wilcox
331 et al., 2015).

332 **3.3.1 Global temperature response**

333 In the experiment where European anthropogenic SO_2 emissions are removed, the global average temperature change per
334 unit emission is approximately twice of that in the 7xEU experiment, as well as in the other experiments where emissions
335 were increased (Fig. 3 and Table 2). The global average temperature change per unit emission in the emission reduction
336 experiment is significantly different from those in the emission increase experiments (Fig. S1). This indicates that there is
337 a non-linearity depending on the magnitude and sign of the emission change, at least for European SO_2 emissions. Since the
338 coupled simulations include aerosol indirect effects, and since indirect effects are usually larger than direct aerosol effects (Rap
339 et al., 2013; Myhre et al., 2013; Kirkevåg et al., 2013), nonlinear effects pertaining to aerosol-cloud interactions most likely
340 play a role in the difference in global climate sensitivity between the 0xEU and 7xEU experiments. However, effects related to
341 the modeled aerosol microphysics could also play a role in this difference, in particular when SO_2 emissions and concentrations

342 are low. For example, in extreme conditions the partitioning between different aerosol microphysical paths might change, like
343 condensation and nucleation rates of sulphate (Stier et al., 2006).

344 The two experiments with different European SO₂ emission perturbations illustrate the difficulties related to the generality
345 of the method of translating emission perturbations to temperature response already discussed in Section 3.1. The global mean
346 temperature responses per unit sulphur emission differ substantially for these two experiments, as well as the magnitudes of
347 the latitudinal and regional temperature responses.

348 We return to the question of "basis quantities" (cf. Sect. 3.1) and for which step in the translation from emission to tem-
349 perature response the largest divergence appears for the different experiments. The normalised global temperature responses
350 per unit emission in the experiments where SO₂ emissions are increased are close to unity, while the normalised temperature
351 response per unit emission in the 0xEU experiment is larger than two (Fig. 3). The translation from emission to column burden
352 for the EU emission changes is not dependent on the emission magnitude in the experiments presented here. Similar to what
353 was noted for the other experiments, the RF per unit emission change in 0xEU and 7xEU is similar to the column burden
354 response per unit emission change. The normalised ERF sensitivity to unit emission perturbation on the other hand, bears more
355 resemblance with the temperature response for the 0xEU and 7xEU experiments (third group of bars/the next rightmost bars
356 in Fig. 3a). This indicates that fast cloud feedbacks, such as cloud lifetime, liquid water content or semidirect effects, is most
357 likely a key component for understanding the non-linearity in the temperature response to European emissions (cf. Table S1
358 and S2).

359 Emission perturbation was in Sect. 3.1 found to be a good predictor of the temperature response for emission increases
360 from all regions investigated when the emissions were increased with similar magnitudes. However, it does not capture the non-
361 linear behaviour in the temperature response to European emission perturbations of different magnitudes (Fig. 3b). Similarly,
362 RF and column burden as basis quantities also fail to capture this property in the response to European emission perturbations.
363 The ERF is the only basis quantity that captures the non-linearity for European emission perturbations of varying magnitude.
364 However, there is substantial variability in the predictability for the temperature responses in the other experiments. The ERF
365 shows the smallest standard deviation for the different basis quantities when all experiments are considered (Table 3), but this
366 is due to substantially larger standard deviations for emissions, CB and RF as basis quantities when the 0xEU experiment is
367 included. Nevertheless, the ERF is the basis quantity with the highest degree of generality for the global results from all the
368 experiments conducted with NorESM presented in this study.

369 3.3.2 Sub-global temperature response

370 Similarly to the global mean response, the magnitude of the latitudinal and regional temperature responses per unit sulphur
371 emission are substantially larger in the 0xEU experiment than in the 7xEU experiment, with the exception for the temperature
372 difference in SA which is not statistically significant compared to the control simulation (Fig. 10, where that hatched bars
373 indicate the 7xEU response for easy comparison). For the latitudinal sensitivities, the pattern of increasing temperature response
374 with latitude found in the experiments where emissions were increased (Sect. 3.2.1 and Fig. 4) is also seen for the 0xEU
375 experiment. The relative impact on the southern hemisphere is also larger in this experiment compared to the other experiments.

376 All latitudinal temperature changes in the 0xEU experiment are significantly different from the responses in all the other
377 experiments except for the tropical latitude band (Fig. S1).

378 The regional 0xEU responses display a similar pattern to the regional responses in the 7xEU experiment, but with different
379 magnitudes. The largest temperature response is seen in the AR region whereas outside AR the largest response is found in the
380 emission region (EU). The temperature responses to reduced EU SO₂ emissions in NA and EA are close to the zonal means
381 for the latitudes covered by these regions (within 2%). This is similar to the the corresponding regional temperature responses
382 in the 7xEU experiment relative to the zonal mean responses.

383 The non-linear effects are mostly confined to the magnitude of the temperature responses in the case for European emission
384 perturbations in these experiments. Zonal asymmetries do not appear to have a significant impact on the regional temperature
385 responses. This might, however, be different for the Asian emission perturbations where zonal asymmetries seem to play a more
386 prominent role in the regional temperature distributions compared to the European and North American emission perturbations.

387 **3.4 Comparison with other RTP coefficients**

388 In this work we have aimed to establish the simplest possible model for anthropogenic aerosol impacts on regional tempera-
389 tures, i.e. an emission-based regional temperature potential coefficient.

390 Nevertheless, difficulties associated with nonlinear effects in this relationship remain where ERF proved to be a more general
391 basis quantity for estimating the global temperature response than emissions, in terms of capturing different magnitudes of
392 global mean temperature responses for different emission changes in Europe.

393 With the experimental set up applied in this study, it is not possible to derive sub-global (latitudinal or regional) radia-
394 tive forcing-based sensitivities, as the forcing changes in the different experiments are not confined to a certain region or
395 latitude band. However, with the latitudinal and regional RF and ERF from the different experiments, the generality of the
396 RTP-coefficients derived by Shindell and Faluvegi (2009) and Shindell (2012) can be assessed for the NorESM generated
397 temperature response. For each experiment the RF and ERF in each latitude band resulting from the regional emission per-
398 turbations are calculated (Table 4) and used with different methods for calculating the latitudinal temperature responses, the
399 ARTP.

400 First we compare the temperature response as calculated from Equations 1 and 2 with that from the simulations with NorESM
401 where SO₂ emissions were increased. Both equations require knowledge of the model global climate sensitivity (or the Impulse
402 Response Function). The climate sensitivities are derived from the emission perturbation experiments, and we use a mean value
403 from all experiments with emission increases. Climate sensitivities for both RF and ERF are derived, and these are calculated
404 to be 0.47 and 0.61 K(Wm⁻²)⁻¹, respectively.

405 However, the model global climate sensitivity is not always known, e.g. if the forcing is derived with a Chemistry Trans-
406 port Model (CTM). Moreover, one motivation behind using RTP coefficients is to avoid conducting multi-century coupled
407 simulation, which is necessary for deriving the climate sensitivity. Therefore, we also evaluate the performance of the RTP
408 coefficients with a standardised climate sensitivity as well as applying the RTP coefficients of Shindell and Faluvegi (2010)
409 as regional sensitivity coefficients (i.e. without normalising with the regional climate sensitivity to global forcing and scaling

410 with the model's global sensitivity). This is to see how well the RTP-method predicts the model temperature response when
411 the specific model's climate sensitivity to a particular forcing agent is unknown.

412 The latitudinal temperature responses calculated from Equations 1 and 2 are shown in Fig. 11 and 12. The small dots indicate
413 the temperature response in specific regions and the filled circles indicate the emission source regions. The high latitude
414 temperature response in the northern hemisphere (ARCT) calculated using the RTP coefficients, the ARTP, is underestimated
415 compared to the temperature response in the NorESM experiments (but still within one standard deviation of the NorESM
416 simulated temperature response), except for when the ERF is used in combination with the normalised coefficients of Shindell
417 et al. (2012) (Fig. 12b). This is also the method that gives the smallest root mean square deviation (RMSD) of 0.14K (RMSDs
418 are displayed in each panel). In general, ERF is a better predictor of the latitudinal temperature response than RF, based on
419 the RMSD. Similarly, the RTP coefficients that are normalised by the global sensitivity (Shindell et al., 2012) rather than the
420 regional sensitivity (Shindell and Faluvegi, 2010), i.e. Fig. 11 vs. Fig. 12, is a better model for the temperature response in each
421 latitude band, also based on the RMSD. This was also pointed out by Shindell (2012).

422 However, the performance of this method relies on that the correct climate sensitivity is used and is known. The standard
423 definition of equilibrium climate sensitivity (ECS) is the equilibrium temperature response to a doubling of CO₂ (Collins
424 et al., 2013), and is available for nearly all models participating in the Coupled Model Intercomparison Project phase 5 (Flato
425 et al., 2013). For NorESM this climate sensitivity has been estimated to 0.91 K/Wm⁻² (Iversen et al., 2013, λ_{reg} in Table
426 1). This is higher than the sensitivity to aerosol forcing obtained in this study. The climate sensitivity from the simulations
427 presented here is not directly comparable with an equilibrium climate sensitivity, since an equilibrium temperature response
428 would require considerably longer simulations for allowing the ocean to fully adjust. The results of the RTP method with this
429 ECS applied is shown in Figure 13. Overall, the use of ECS overestimates the temperature response in almost all latitude bands.
430 Thus, it is important to use a climate sensitivity appropriate for the time scale investigated and possibly also for the particular
431 climate forcer in question. This is a complicating factor since it requires a priori knowledge of this quantity, which can only be
432 derived by performing coupled simulations, the necessity of which one often would like to eliminate with a simplified method.
433 Moreover, if calculations to derive radiative forcing are performed with a CTM, this quantity is not available.

434 A third alternative is to apply the RTP coefficients without normalising with a model dependent climate sensitivity parameter,
435 i.e. using the RTP-coefficients of Shindell and Faluvegi (2010), Table 3, directly with forcing estimates (Fig. 14). The implicit
436 assumption in this method is that the sensitivity of NorESM to aerosol forcing is equal to that of the GISS model simulations
437 used to derive the RTP coefficient. This is equivalent with applying the GISS model's sensitivity of 0.5 K/Wm⁻² (Shindell,
438 2012) in Equation 2. This assumption about the sensitivity leads to RTP-derived temperature responses with smaller RMSD
439 values than both those derived by applying the ECS for NorESM in Equation 1 and 2.

441 **4.1 Uncertainties associated with RTP coefficients**

442 The method applied in this work, i.e. evaluating the global and regional temperature responses based on the emission change
443 magnitudes, means that on the one hand, the starting quantity is easy to assess and compare and is easy to incorporate into
444 integrated assessment models, such as GAINS. The full response chain from emissions to atmospheric concentrations, to forc-
445 ing, to surface temperature response is accounted for in this metric. On the other hand, the fact that the metric encompasses
446 the full chain from emission to temperature response means that there are implicit uncertainties in the metric. The representa-
447 tiveness of these emission based RTP coefficients will depend on how well the climate model used to derive these coefficients,
448 represents a large number of atmospheric chemical and physical processes on many different spatial and temporal scales. The
449 RTP coefficients derived by Shindell and Faluvegi (2009) and Shindell (2012) were derived from radiative forcing, and thus
450 do not contain the uncertainties introduced when estimating the column burden and forcing associated with aerosol emissions.
451 However, a model to translate emission to radiative forcing, either RF or ERF, is still necessary to make these forcing based
452 RTP coefficients useful in an integrated assessment modelling context based on emission pathways.

453 Some major uncertainties can be identified if the emission-temperature response chain is broken down into sub steps. First,
454 emissions of an atmospheric chemical compound result in an atmospheric concentration and column burden. The translation
455 from emission of an atmospheric chemical component to atmospheric aerosol loading depends on a number of factors, e.g. if the
456 aerosol originates from primary emission or is formed through chemical reactions in the atmosphere (i.e. secondary aerosols),
457 like sulphate which is studied here. The aerosol production for secondary aerosols will depend on which and how chemical
458 reactions that produce these aerosols are described in the atmospheric model. Kasoar et al. (2016) found that the efficiency of
459 chemical conversion of SO₂ to sulphate was one process contributing to differences in the simulated responses in three different
460 climate models to equivalent emission reductions over China. In addition to chemical production, the interaction with clouds
461 will influence the atmospheric concentration of aerosols. Wet removal through precipitation is an efficient removal process
462 for hygroscopic aerosols like sulphate containing compounds. All these factors, emission strength, atmospheric production
463 and removal efficiency influence how long aerosol particles stay in the atmosphere and how far they are transported from the
464 emission sources. Thus, all these processes influence the atmospheric loading and how these processes are represented in the
465 model will influence the modelled aerosol column burden.

466 Another source of uncertainty in the emission-forcing-temperature chain, besides the modelled column burden, is how the
467 aerosol radiative properties are modelled (Myhre et al., 2013). The radiative properties of aerosols depend on e.g. their chemical
468 composition, water content and mixing state. Thus, given the same atmospheric concentration and distribution of aerosols, their
469 radiative effect might vary depending on how their radiative properties are represented in the model. Other complicating factors
470 when it comes to aerosol radiative effects are clouds and aerosol indirect and semi-direct effects on clouds. The direct radiative
471 forcing will depend on the cloud distribution itself, and aerosol can affect the properties of clouds and also, affect the cloud
472 distribution, i.e. other components, besides the aerosol itself, within the model influence their radiative effects (Stier et al.,
473 2013).

474 One of the largest uncertainties associated with the effect of aerosols on climate is related to their indirect effect on clouds
475 (Myhre et al., 2013) and the representation of these can vary widely between different models. Beside chemical conversion
476 and radiative impacts, Kasoar et al. (2016) also identified indirect effects on clouds as a major source of diversity between the
477 models they investigated. Wilcox et al. (2015) found that parameterisations of the relationship between cloud droplet number
478 concentration and effective radius was the largest contribution to differences in the cloud albedo effect between three models
479 from the CMIP5 archive, among those NorESM.

480 The factors described above all contribute to inter-model diversity, and will influence how general RTP coefficients are
481 across models. However, the same processes also contribute to regional sensitivity differences within the same model, but not
482 based on differences in how the processes are represented in the model, but on the specific meteorological conditions in each
483 region (e.g. cloud climatology, regional circulation patterns and the background aerosol).

484 The results presented in this study indicate that the temperature sensitivity depends on the emission change magnitude in
485 NorESM. The global temperature response per unit SO₂ emission in the EU SO₂ removal experiment is approximately twice of
486 that in the EU SO₂ increase experiment, although the results are also associated with large uncertainties. The nonlinearity in
487 the response appears to belong to aerosol interactions with clouds and in particular to fast feedbacks included in the ERF. These
488 include changes in liquid water content, cloud fraction and subsequent changes in cloud albedo of the new cloud distribution,
489 i.e. cloud life time effects (Albrecht, 1989) (the cloud albedo effect of the background cloud distribution is included in RF).

490 Wilcox et al. (2015) derived simple functional forms representing the relationship between sulphate load and cloud droplet
491 effective radius (i.e. the cloud albedo effect) in three different CMIP5 models, with which they could reproduce the time
492 evolution of the simulated cloud droplet effective radius from historical 20th century simulations. With these functional forms,
493 they could also quantify the intrinsic varying sensitivity in the parameterisation of the effective radius which depends on the
494 magnitude of the sulphate load, and how the effective radius (and ultimately radiative forcing) goes from being highly sensitive
495 at low sulphate loads to a relative insensitive state at high sulphate loads. While they focussed on the cloud albedo effect, the
496 cloud life time effect is a direct consequence of initial change in effective radius, and should thus display a similar varying
497 sensitivity depending on the absolute sulphate load.

498 Thus, the similarity of the global temperature responses in the emission increase experiments, despite different mechanisms,
499 might be due to this saturation of cloud droplet effective radius change when emission increases are large enough. The tem-
500 perature sensitivity for the different regions could prove to be different if emission were reduced, even by equivalent amounts,
501 depending on the regional background emission strength and regional meteorological conditions. Nonlinear effects depending
502 on the emission change magnitude and background is one of the biggest hurdles in creating a general emission based RTP
503 coefficient.

504 **4.2 Basis quantity**

505 Different quantities for predicting the temperature response have been assessed for the global mean temperature and for latitu-
506 dinal bands in combination with the RTP coefficients of Shindell and Faluvegi (2010) and Shindell (2012). In both cases ERF
507 proved to have the best skill to predict the temperature response.

508 For the global mean temperature response, the ERF was the only variable that was capable of capturing the large difference
509 in the temperature responses to the European increase and decrease in SO₂ emissions. However, for the emission increase
510 experiments, emission change was a good predictor for temperature change. Also for the latitudinal ARTPs the ERF performed
511 better in predicting temperature responses than the RF for NorESM, which is mostly due to a simulated larger ERF than RF in
512 the Arctic region. This can either be an indication that the sensitivity of the Arctic region is larger in NorESM than GISS to
513 forcing outside the Arctic region, i.e. that the coefficient relating the forcing to Arctic temperature responses should be larger
514 for NorESM. It could also be an indication that the cloud feedbacks in the Arctic is a necessary part of the forcing, and that the
515 local forcing from fast feedbacks is important for the Arctic response in NorESM.

516 4.3 Latitudinal and regional sensitivities

517 The sensitivity of zonal mean temperatures to emission perturbations in different regions show large similarities, with the
518 exception of the overall weaker northern hemisphere temperature response to SA SO₂ emissions; the zonal mean temperature
519 change increase with increasing latitude in all experiments and do not appear to depend strongly on the location of the emission
520 perturbations within the northern hemisphere (Fig. 4). There are many factors that might contribute to the weaker temperature
521 response to the SA emission perturbation. This emission perturbation is located in one of the major monsoonal regions on the
522 globe, and the increase of sulphate leads to a substantial reduction of precipitation over SA (Table S1 and S2). The reduced
523 precipitation, in turn, leads to less efficient wet removal of aerosol resulting in an increased residence time and a larger column
524 burden response per unit emission of both sulphate and BC compared to the control simulation. The decrease in precipitation
525 in SA (as well as smaller increases in liquid water path, Table S1 and S2) also contribute to a weaker ERF and indirect effect
526 on clouds, which, in the other experiments enhances the local forcing, but not in SA (Fig. 9). This result is one example of how
527 different local meteorological conditions where the emission changes occur contribute to different forcing and temperature
528 responses within the same model.

529 The general pattern, which indicates a stronger temperature response with increasing latitude for all emission perturbations,
530 is a robust feature in all experiments. In all experiments, the second largest regional sensitivity (after the Arctic region), is
531 generally found in the region of the emission perturbation. However, for SA emissions, the sensitivity is slightly larger in the
532 East Asian region compared to the South Asian emission region, a result caused by production of sulphate aerosol from SO₂
533 and subsequent transport from SA to EA. These results are in line with those of Conley et al. (2018), who found a similar
534 latitudinal temperature change distribution in three different models in response to removal of US SO₂ emissions, and Kasoar
535 et al. (2018) who conducted a single model study where they found that the Arctic warmed most in response to removal of SO₂
536 emissions in different regions.

537 Moreover, Asian SO₂ emissions, both from EA and SA, produce larger zonal asymmetries in the global temperature change
538 field than those of EU and NA. The Asian SO₂ emissions lead to temperature responses in NA and EU that are higher and
539 lower, respectively, than the zonal mean response. The remote regional temperature responses to EU and NA SO₂ emissions are
540 on the other hand close to the corresponding zonal mean responses. The location in the Asian monsoon region and proximity
541 to the Western Pacific mean that these SO₂ emissions could cause tropical precipitation changes that are effective in generating

542 planetary scale waves. These waves can propagate into the extratropics, which in turn influences the global temperature distri-
543 bution (Ming et al., 2011; Lewinschal et al., 2013). Moreover, Teng et al. (2012) found a temperature impact in North America
544 directly linked to absorbing aerosols in Asia.

545 However, the standard deviations for the regional sensitivities are larger than those for the latitudinal sensitivities and zonal
546 mean sensitivities. Nevertheless, despite the larger uncertainties associated with the regional RTPs compared to the latitudinal
547 RTPs, they provide information that is not captured by the latitudinal RTPs.

548 **5 Summary and Conclusions**

549 We performed simulations with the Earth system model NorESM to evaluate the surface temperature change in response to
550 SO₂ emission perturbations in Europe, North America and East and South Asia, and to derive emission-based RTP coefficients.
551 Four experiments were performed where emissions were increased relative to the year 2000 in each individual region to yield
552 similar global mean radiative forcing values. One additional experiment was performed where anthropogenic SO₂ emissions
553 were completely removed in Europe.

554 In all five experiments the zonal mean latitudinal temperature change distribution showed a similar pattern of increasing
555 temperature change with increasing latitude, independently of where the emission perturbation was located. The largest tem-
556 perature response in all experiments performed was in this study thus found in the Arctic region, no matter where the emission
557 perturbations were located, similarly to the result of Conley et al. (2018) and Kasoar et al. (2018). Outside the Arctic region, the
558 temperature response was largest in the emission perturbation region, except for SA emissions where the temperature response
559 in the neighbouring EA region was equally large. This result was consistent with the radiative forcing pattern, which was also
560 strongest in the emission region in each experiment.

561 Furthermore, indications were found that the emission-based RTPs derived with NorESM might be non-linear. Removal
562 of anthropogenic European SO₂ emissions led to a temperature response per unit emission approximately twice of that in
563 the 7xEU experiment in NorESM. The result is, however, associated with large uncertainties. Other differences were also
564 noticed for the regional responses to regional emission perturbations. Asian emission increases led to a different remote effect
565 compared to increases in EU and NA emissions. Both EA and SA emission perturbations led to a NA temperature response that
566 was larger than the zonal mean and an EU response that was smaller than the corresponding zonal mean. EU and NA emission
567 perturbations, on the other hand, led to remote responses that were close to the zonal mean for the same latitudes.

568 A comparison of the modelled temperature response in NorESM with that calculated using ARTPs (equations 1 and 2)
569 derived with the RTP coefficients of Shindell and Faluvegi (2010) and Shindell (2012) showed that the RTP coefficients predict
570 similar latitudinal temperature change distributions as those produced by NorESM. The agreement between the calculated
571 values using ARTPs and the temperature change simulated using NorESM was better when ERF was used together with the
572 RTP coefficient than when RF was used. This was mainly due to a larger Arctic ERF than RF that resulted in an Arctic
573 temperature response closer to that produced in the NorESM simulations. This result could be an indication that the Arctic is

574 more sensitive to forcing outside this region in NorESM than in the GISS model, or that local fast cloud feedbacks are crucial
575 for the Arctic temperature response in NorESM.

576 Even though the global mean temperature response to emission increases is similar in all regions, the processes leading to
577 the change may be different in different regions, as it depends on the local meteorological conditions. In all regions except SA,
578 aerosol indirect effects on clouds, and particularly life time effects, are dominating the ERF response. For SA, direct radiative
579 effects have a higher relative importance in the response since the local responses in cloud fraction, liquid water path and
580 precipitation are either weaker compared to the other emission regions or decrease in response to increased SO₂ emissions.
581 The latitudinal distribution of the zonal mean temperature response to SA emission changes also differs from the rest of the
582 simulations in that the Northern hemisphere response is weaker and the southern hemisphere and tropical responses are stronger
583 than in the other simulations.

584 Air pollution globally cause more than 4 million premature deaths each year and as sulphates are major air pollution com-
585 ponents, emission reductions of SO₂ will be absolutely necessary to improve air quality. The derived emission-based RTPs
586 will simplify development of cost effective co-beneficial abatement strategies that can give both better air quality and mitigate
587 climate change. The nonlinear effect predicted by NorESM indicate a reduced immediate climate effect of SO₂ emission re-
588 ductions in highly polluted areas where the indirect effect is saturated but the effect would become more evident with time as
589 the saturation of aerosol indirect effects diminishes. Nevertheless, emission reductions of SO₂ and other short-lived climate
590 forcers are necessary for improving air quality and public health in both Europe, North America and Asia.

591 *Author contributions.* AL, AMLE, HCH, MS, TKB and JL designed the experiments. AL carried out the simulations. AL prepared the
592 manuscript with contributions from all co-authors.

593 *Competing interests.* The authors declare that they have no conflict of interest.

594 *Acknowledgements.* This work was supported by the Swedish Environmental Protection Agency through the Swedish Clean Air and Climate
595 research program (SCAC) and the Research Council of Norway through the EVA (grant 229771). The NorESM simulations were performed
596 on resources provided by the Swedish National Infrastructure for Computing (SNIC) at the National Supercomputer Centre (NSC). We thank
597 two anonymous reviewers for their helpful comments.

598 References

- 599 Aamaas, B., Peters, G. P., and Fuglestedt, J. S.: Simple emission metrics for climate impacts, *Earth System Dynamics*, 4, 145–170,
600 <https://doi.org/10.5194/esd-4-145-2013>, 2013.
- 601 Acosta Navarro, J. C., Varma, V., Riipinen, I., Seland, O., Kirkevåg, A., Struthers, H., Iversen, T., Hansson, H. C., and Ekman, A. M. L.:
602 Amplification of Arctic warming by past air pollution reductions in Europe, *Nature Geosci.*, 9, <https://doi.org/10.1038/NGEO2673>, 2016.
- 603 Albrecht, B.: Aerosols, cloud microphysics, and fractional cloudiness, *Science*, 245, 1227–1230,
604 <https://doi.org/10.1126/science.245.4923.1227>, 1989.
- 605 Amann, M., Bertok, I., Borcken-Kleefeld, J., Cofala, J., Heyes, C., Hoeglund-Isaksson, L., Klimont, Z., Nguyen, B., Posch, M., Rafaj, P.,
606 Sandler, R., Schoepp, W., Wagner, F., and Winiwarter, W.: Cost-effective control of air quality and greenhouse gases in Europe: Modeling
607 and policy applications, *Environmental Modelling & Software*, 26, 1489–1501, <https://doi.org/10.1016/j.envsoft.2011.07.012>, 2011.
- 608 Bellouin, N., Baker, L., Hodnebrog, O., Olivie, D., Cherian, R., Macintosh, C., Samset, B., Esteve, A., Aamaas, B., Quaas, J., and Myhre, G.:
609 Regional and seasonal radiative forcing by perturbations to aerosol and ozone precursor emissions, *Atmospheric Chemistry and Physics*,
610 16, 13 885–13 910, <https://doi.org/10.5194/acp-16-13885-2016>, 2016.
- 611 Bentsen, M., Bethke, I., Debernard, J. B., Iversen, T., Kirkevåg, A., Seland, O., Drange, H., Roelandt, C., Seierstad, I. A., Hoose, C., and
612 Kristjansson, J. E.: The Norwegian Earth System Model, NorESM1-M - Part 1: Description and basic evaluation of the physical climate,
613 *Geoscientific Model Development*, 6, 687–720, <https://doi.org/10.5194/gmd-6-687-2013>, 2013.
- 614 Collins, M., Knutti, R., Arblaster, J., Dufresne, J.-L., Fichetef, T., Friedlingstein, P., Gao, X., Gutowski, W., Johns, T., Krinner, G., Shongwe,
615 M., Tebaldi, C., Weaver, A., and Wehner, M.: Long-term Climate Change: Projections, Commitments and Irreversibility., In: *Climate
616 Change 2013: The Physical Science Basis. Contribution of Working Group I to the Fifth Assessment Report of the Intergovernmental
617 Panel on Climate Change* [Stocker, T.F., D. Qin, G.-K. Plattner, M. Tignor, S.K. Allen, J. Boschung, A. Nauels, Y. Xia, V. Bex and P.M.
618 Midgley (eds.)]. Cambridge University Press, Cambridge, United Kingdom and New York, NY, USA., 2013.
- 619 Conley, A. J., Westervelt, D. M., Lamarque, J. F., Fiore, A. M., Shindell, D., Correa, G., Faluvegi, G., and Horowitz, L. W.: Multimodel
620 Surface Temperature Responses to Removal of US Sulfur Dioxide Emissions, *Journal of Geophysical Reserach-Atmospheres*, 123, 2773–
621 2796, <https://doi.org/10.1002/2017JD027411>, 2018.
- 622 Dong, B., Sutton, R. T., Highwood, E. J., and Wilcox, L. J.: Preferred response of the East Asian summer monsoon to local and non-local
623 anthropogenic sulphur dioxide emissions, *Climate Dynamics*, 46, 1733–1751, <https://doi.org/10.1007/s00382-015-2671-5>, 2016.
- 624 Flato, G., Marotzke, J., Abiodun, B., Braconnot, P., Chou, S., Collins, W., Cox, P., Driouech, F., Emori, S., Eyring, V., Forest, C., Gleckler,
625 P., Guilyardi, E., Jakob, C., Kattsov, V., Reason, C., and Rummukainen, M.: Evaluation of Climate Models., In: *Climate Change 2013:
626 The Physical Science Basis. Contribution of Working Group I to the Fifth Assess- ment Report of the Intergovernmental Panel on Climate
627 Change* [Stocker, T.F., D. Qin, G.-K. Plattner, M. Tignor, S.K. Allen, J. Boschung, A. Nauels, Y. Xia, V. Bex and P.M. Midgley (eds.)].
628 Cambridge University Press, Cambridge, United Kingdom and New York, NY, USA., 2013.
- 629 Iversen, T., Bentsen, M., Bethke, I., Debernard, J. B., Kirkevåg, A., Seland, O., Drange, H., Kristjansson, J. E., Medhaug, I., Sand, M., and
630 Seierstad, I. A.: The Norwegian Earth System Model, NorESM1-M - Part 2: Climate response and scenario projections, *Geoscientific
631 Model Development*, 6, 389–415, <https://doi.org/10.5194/gmd-6-389-2013>, 2013.
- 632 Kasoar, M., Voulgarakis, A., Lamarque, J.-F., Shindell, D., Bellouin, N., Collins, W., Faluvegi, G., and Tsigaridis, K.: Regional and global
633 temperature response to anthropogenic SO₂ emissions from China in three climate models, *Atmospheric Chemistry and Physics*, 16,
634 9785–9804, <https://doi.org/10.5194/acp-16-9785-2016>, <http://dx.doi.org/10.5194/acp-16-9785-2016>, 2016.

635 Kasoar, M., Shawki, D., and Voulgarakis, A.: Similar spatial patterns of global climate response to aerosols from different regions, *npj*
636 *Climate and Atmospheric Science*, 1, <https://doi.org/https://doi.org/10.1038/s41612-018-0022-z>, 2018.

637 Kirkevåg, A., Iversen, T., Seland, O., Hoose, C., Kristjánsson, J. E., Struthers, H., Ekman, a. M. L., Ghan, S., Griesfeller, J., Nilsson, E. D.,
638 and Schulz, M.: Aerosol-climate interactions in the Norwegian Earth System Model - NorESM1-M, *Geoscientific Model Development*,
639 6, 207–244, <https://doi.org/10.5194/gmd-6-207-2013>, 2013.

640 Lamarque, J.-F., Bond, T. C., Eyring, V., Granier, C., Heil, A., Klimont, Z., Lee, D., Liousse, C., Mieville, A., Owen, B., Schultz, M. G.,
641 Shindell, D., Smith, S. J., Stehfest, E., Aardenne, J. V., Cooper, O. R., Kainuma, M., Mahowald, N., McConnell, J. R., Naik, V., Riahi,
642 K., and van Vuuren, D. P.: Historical (1850-2000) gridded anthropogenic and biomass burning emissions of reactive gases and aerosols:
643 methodology and application, *Atmospheric Chemistry and Physics*, 10, 7017–7039, doi:10.1029/2007GL030541, 2010.

644 Lewinschal, A., Ekman, A. M. L., and Kornich, H.: The role of precipitation in aerosol-induced changes in northern hemisphere wintertime
645 stationary waves, *Climate Dynamics*, 41, 647–661, <https://doi.org/10.1007/s00382-012-1622-7>, 2013.

646 Menon, S., Hansen, J., Nazarenko, L., and Luo, Y.: Climate effects of black carbon aerosols in China and India, *Science*, 297, 2250–2253,
647 2002.

648 Ming, Y., Ramaswamy, V., and Chen, G.: A model investigation of aerosol-induced changes in boreal winter extratropical circulation, *Journal*
649 *of Climate*, 24, 6077–6091, doi: 10.1175/2011JCLI4111.1, 2011.

650 Myhre, G., Shindell, D., Bréon, F.-M., Collins, W., Fuglestedt, J., Huang, J., Koch, D., Lamarque, J.-F., Lee, D., Mendoza, B., Nakajima,
651 T., Robock, A., Stephens, G., Takemura, T., and Zhang, H.: Anthropogenic and Natural Radiative Forcing., In: *Climate Change 2013:*
652 *The Physical Science Basis. Contribution of Working Group I to the Fifth Assessment Report of the Intergovernmental Panel on Climate*
653 *Change* [Stocker, T.F., D. Qin, G.-K. Plattner, M. Tignor, S.K. Allen, J. Boschung, A. Nauels, Y. Xia, V. Bex and P.M. Midgley (eds.)].
654 Cambridge University Press, Cambridge, United Kingdom and New York, NY, USA, 2013.

655 Myhre, G., Samset, B. H., Schulz, M., Balkanski, Y., Bauer, S., Berntsen, T. K., Bian, H., Bellouin, N., Chin, M., Diehl, T., Easter, R. C.,
656 Feichter, J., Ghan, S. J., Hauglustaine, D., Iversen, T., Kinne, S., Kirkevåg, A., Lamarque, J. F., Lin, G., Liu, X., Lund, M. T., Luo, G.,
657 Ma, X., van Noije, T., Penner, J. E., Rasch, P. J., Ruiz, A., Seland, O., Skeie, R. B., Stier, P., Takemura, T., Tsigaridis, K., Wang, P., Wang,
658 Z., Xu, L., Yu, H., Yu, F., Yoon, J. H., Zhang, K., Zhang, H., and Zhou, C.: Radiative forcing of the direct aerosol effect from AeroCom
659 Phase II simulations, *Atmospheric Chemistry and Physics*, 13, 1853–1877, <https://doi.org/10.5194/acp-13-1853-2013>, 2013.

660 Rap, A., Scott, C. E., Spracklen, D. V., Bellouin, N., Forster, P. M., Carslaw, K. S., Schmidt, A., and Mann, G.: Natural aerosol direct and
661 indirect radiative effects, *Geophysical Research Letters*, 40, 3297–3301, <https://doi.org/10.1002/grl.50441>, 2013.

662 Shindell, D. and Faluvegi, G.: Climate response to regional radiative forcing during the twentieth century, *Nature Geoscience*, 2, 294–300,
663 <https://doi.org/10.1038/NGEO473>, 2009.

664 Shindell, D. and Faluvegi, G.: The net climate impact of coal-fired power plant emissions, *Atmospheric Chemistry and Physics*, 10, 3247–
665 3260, 2010.

666 Shindell, D., Schulz, M., Ming, Y., Takemura, T., Faluvegi, G., and Ramaswamy, V.: Spatial scales of climate response to inhomogeneous
667 radiative forcing, *Journal of Geophysical Research-Atmospheres*, 115, <https://doi.org/10.1029/2010JD014108>, 2010.

668 Shindell, D. T.: Evaluation of the absolute regional temperature potential, *Atmospheric Chemistry and Physics*, 12, 7955–7960,
669 <https://doi.org/10.5194/acp-12-7955-2012>, 2012.

670 Shindell, D. T., Lamarque, J.-F., Schulz, M., Flanner, M., Jiao, C., Chin, M., Young, P., Lee, Y. H., Rotstajn, L., Milly, G., Faluvegi, G.,
671 Balkanski, Y., Collins, W. J., Conley, A. J., Dalsoren, S., Easter, R., Ghan, S., Horowitz, L., Liu, X., Myhre, G., Nagashima, T., Naik, V.,

672 Rumbold, S., Skeie, R., Sudo, K., Szopa, S., Takemura, T., Voulgarakis, A., and Yoon, J.-H.: Radiative forcing in the ACCMIP historical
673 and future climate simulations, *Atmospheric Chemistry and Physics*, <https://doi.org/doi:10.5194/acpd-12-21105-2012>, 2012.

674 Shine, K., Berntsen, T., Fuglestedt, J., and Sausen, R.: Scientific issues in the design of metrics for inclusion of oxides of nitrogen in global
675 climate agreements, *PNAS*, 102, 15 768–15 773, <https://doi.org/10.1073/pnas.0506865102>, 2005.

676 Stier, P., Feichter, J., Kloster, S., Vignati, E., and Wilson, J.: Emission-induced nonlinearities in the global aerosol system: Results from the
677 ECHAM5-HAM aerosol-climate model, *Journal of Climate*, 19, 3845–3862, <https://doi.org/10.1175/JCLI3772.1>, 2006.

678 Stier, P., Schutgens, N. A. J., Bellouin, N., Bian, H., Boucher, O., Chin, M., Ghan, S., Huneeus, N., Kinne, S., Lin, G., Ma, X., Myhre, G.,
679 Penner, J. E., Randles, C. A., Samset, B., Schulz, M., Takemura, T., Yu, F., Yu, H., and Zhou, C.: Host model uncertainties in aerosol
680 radiative forcing estimates: results from the AeroCom Prescribed intercomparison study, *Atmospheric Chemistry and Physics*, 13, 3245–
681 3270, <https://doi.org/10.5194/acp-13-3245-2013>, 2013.

682 Teng, H., Washington, W. M., Branstator, G., Meehl, G. A., and Lamarque, J.-F.: Potential impacts of Asian carbon aerosols on future US
683 warming, *Geophysical Research Letters*, 39, <https://doi.org/10.1029/2012GL051723>, 2012.

684 Wilcox, L. J., Highwood, E. J., Booth, B. B. B., and Carslaw, K. S.: Quantifying sources of inter-model diversity in the cloud albedo effect,
685 *Geophysical Research Letters*, 42, 1568–1575, <https://doi.org/10.1002/2015GL063301>, 2015.

Table 1. Latitudinal bands definition and region definitions.

Name	Latitudes or region definition
SHext	90°S-28°S
Tropics	28°S-28°N
NHml	28°N-60°N
ARCT	60°N-90°N
AR	66°N-90°N
EU	Europe - HTAPv2
NA	North America - HTAPv2
EA	East Asia - HTAPv2
SA	South Asia - HTAPv2

Table 2. Global results from the experiment where SO₂ emissions in different regions are changed. Units are 10⁻²K/TgSyr⁻¹ for temperature change per emission change, 10⁻²Wm⁻²/TgSyr⁻¹ for RF and ERF per emission change and K/Wm⁻² for temperature change per unit RF and ERF. Standard deviations are in parentheses.

Experiment	0xEU SO ₂	7xEU SO ₂	5xNA SO ₂	5xEA SO ₂	10xSA SO ₂
$\Delta T/\Delta em$	-1.28(1.72)	-0.56(0.32)	-0.61(0.40)	-0.58(0.29)	-0.58(0.45)
RF/ Δem	-1.30(0.02)	-1.04(0.02)	-1.22(0.04)	-1.14(0.04)	-1.68(0.01)
ERF/ Δem	-2.55(0.04)	-0.78(0.75)	-1.29(1.03)	-1.00(0.87)	-0.88(1.08)
$\Delta T/RF$	0.99(1.33)	0.54(0.31)	0.50(0.32)	0.51(0.26)	0.35(0.27)
$\Delta T/ERF$	0.50(1.27)	0.72(0.67)	0.47(0.46)	0.58(0.54)	0.66(0.87)

Table 3. Standard deviations for the different normalised basis quantities evaluated in Figure 3b (unitless).

Variable	EM	RF	ERF	CB
Increased emissions	0.03	0.15	0.19	0.17
All experiments	0.46	0.43	0.19	0.51

Table 4. Regional radiative forcing (RF) and effective radiative forcing (ERF) in Wm^{-2} used to derive latitudinal ARTPs in Fig. 11-14.

Experiment	0xEU SO ₂	7xEU SO ₂	5xNA SO ₂	5xEA SO ₂	10xSA SO ₂
RF					
SH	0.000	-0.003	-0.003	-0.024	-0.038
TROP	0.037	-0.239	-0.224	-0.388	-0.685
NHml	0.329	-1.423	-1.415	-1.315	-0.729
ARCT	0.171	-0.859	-0.488	-0.413	-0.143
ERF					
SH	0.729	0.608	0.663	0.511	0.628
TROP	0.081	-0.170	-0.415	-0.330	-0.489
NHml	-0.184	-1.774	-1.710	-1.752	-0.904
ARCT	-0.139	-1.046	-0.900	-1.075	-0.149

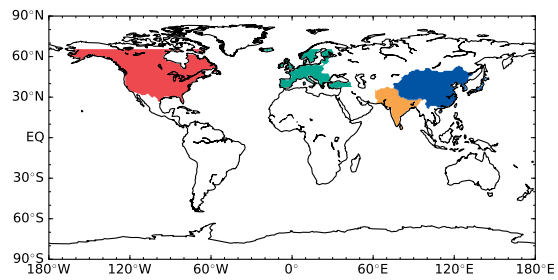


Figure 1. Emission regions according to the HTAP definition. The colours represent: green - Europe (EU), red - North America (NA), blue - East Asia (EA) and yellow - South Asia (SA).

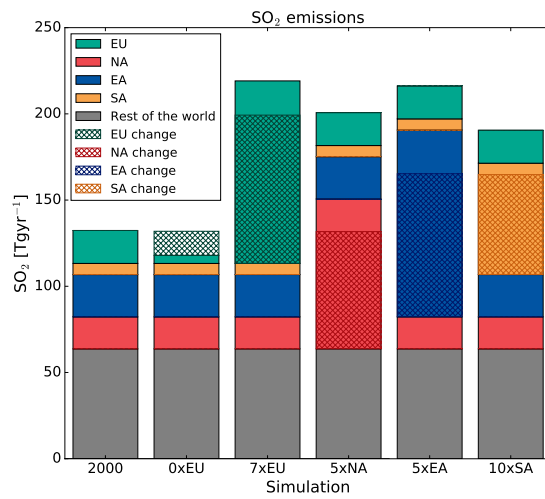


Figure 2. Global annual SO₂ and regional emissions and emission differences in the simulations. Each column shows the total global SO₂ emissions in each simulation and the colour shading indicates the contribution from each region. Hatching indicates the emission change relative to the year 2000 simulation.

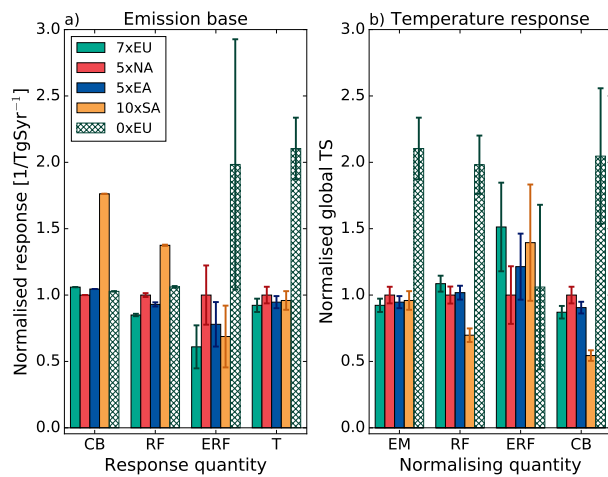


Figure 3. Normalised a) column burden (CB), radiative forcing (RF), effective radiative forcing (ERF) and temperature (T) per unit SO₂ emission, and b) normalised temperature response per emissions, RF, ERF and CB in the different experiments. Quantities are normalised by the 5xNA response. The error bars show the standard error.

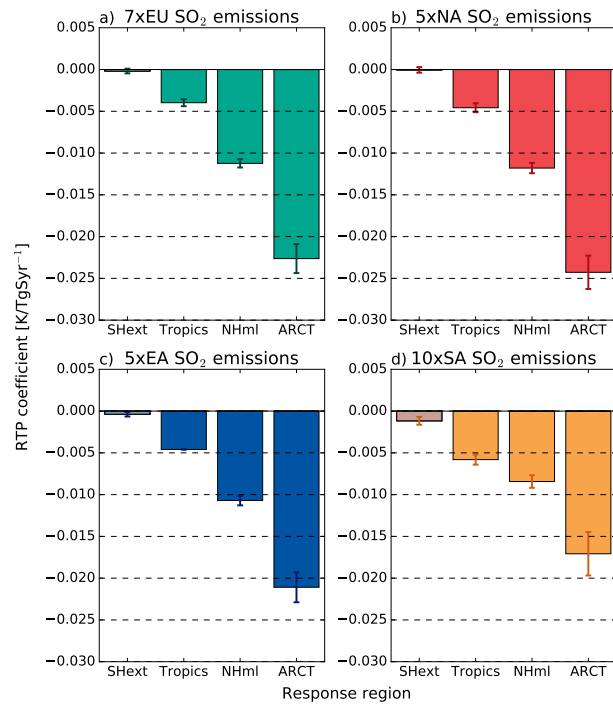


Figure 4. Latitudinal RTP coefficients for SO₂ emission [K/TgSyr⁻¹] for a) EU emissions b) NA emissions c) EA emissions and d) SA emissions. Grey shading indicates that the temperature change is not statistically significant ($p > 0.05$) compared to the control simulation. The error bars show the standard error.

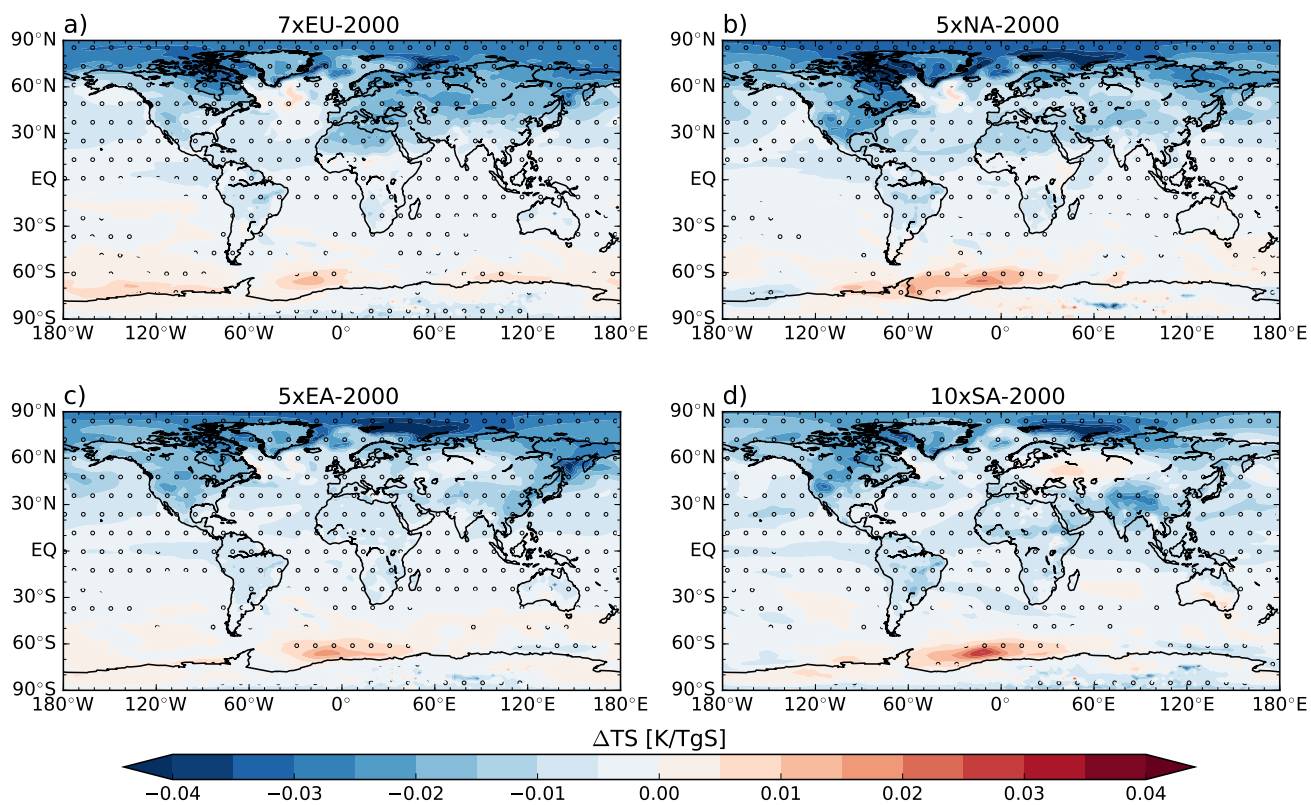


Figure 5. Global temperature change per unit SO₂ emission for a) 7xEU, b) 5xNA, c) 5xEA, d) 10xSA compared to the control simulation. Dots indicate where the result is statistically significant at the 95% confidence level.

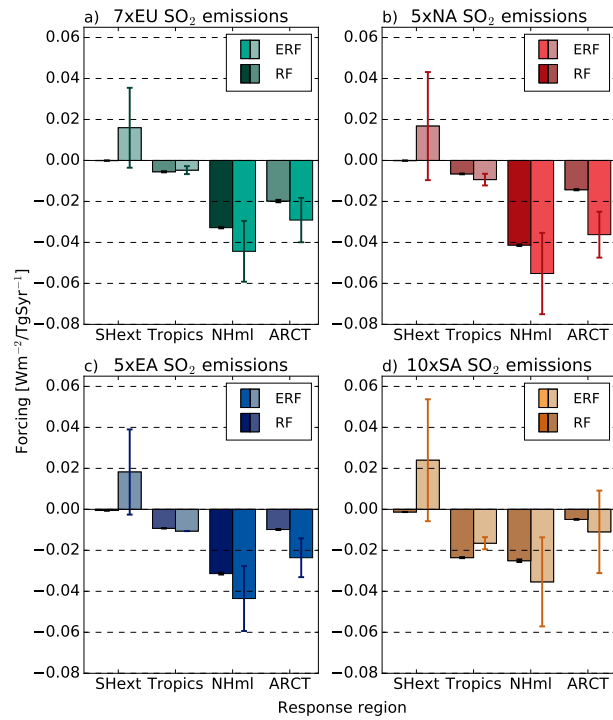


Figure 6. Latitudinal RF and ERF for SO₂ emission [Wm⁻²/TgSyr⁻¹] for a) EU emissions b) NA emissions c) EA emissions and d) SA emissions. In each pair of bars the left bar indicated RF and the right bar indicated ERF. Grey shading indicates that the forcing response is not statistically significant ($p > 0.05$) compared to the control simulation. The error bars show the standard error.

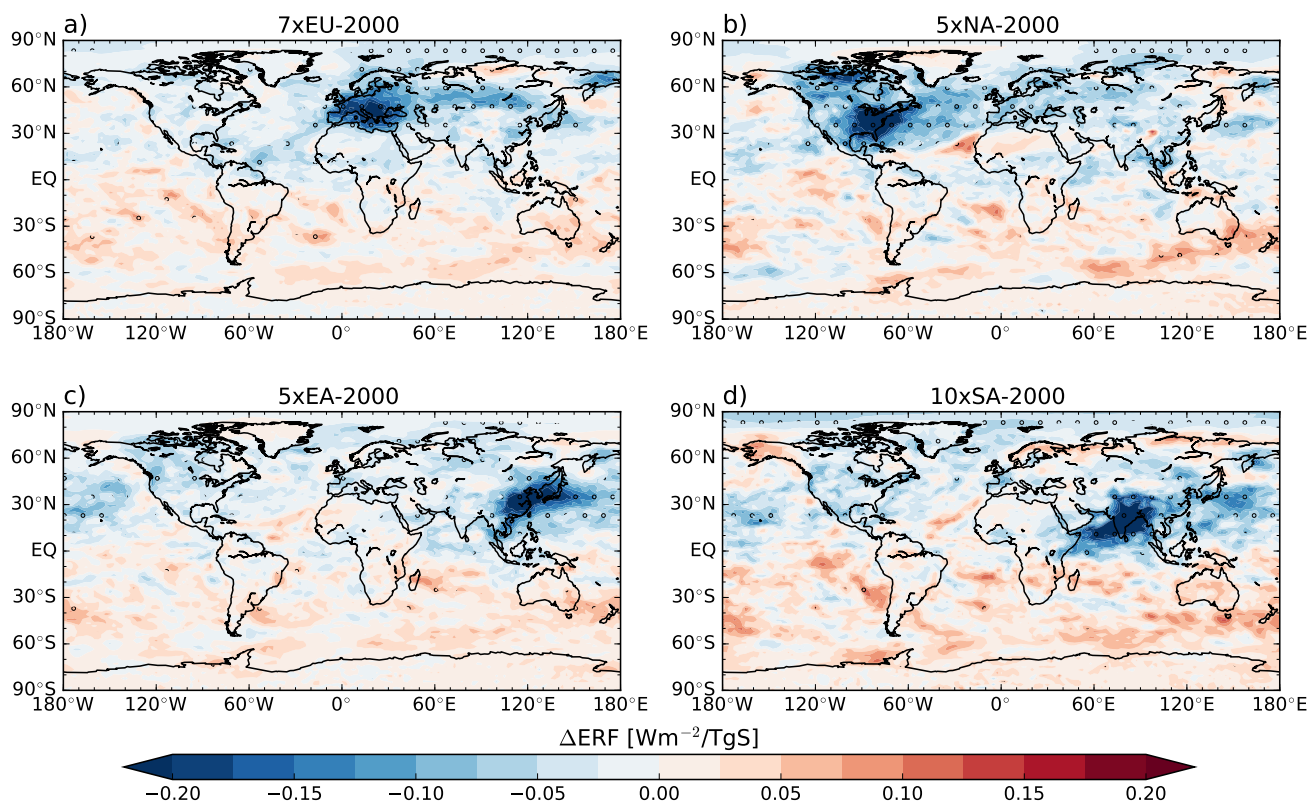


Figure 7. Global effective radiative forcing per unit SO₂ emission for a) 7xEU, b) 5xNA, c) 5xEA, d) 10xSA compared to the control simulation. Dots indicate where the result is statistically significant at the 95% confidence level.

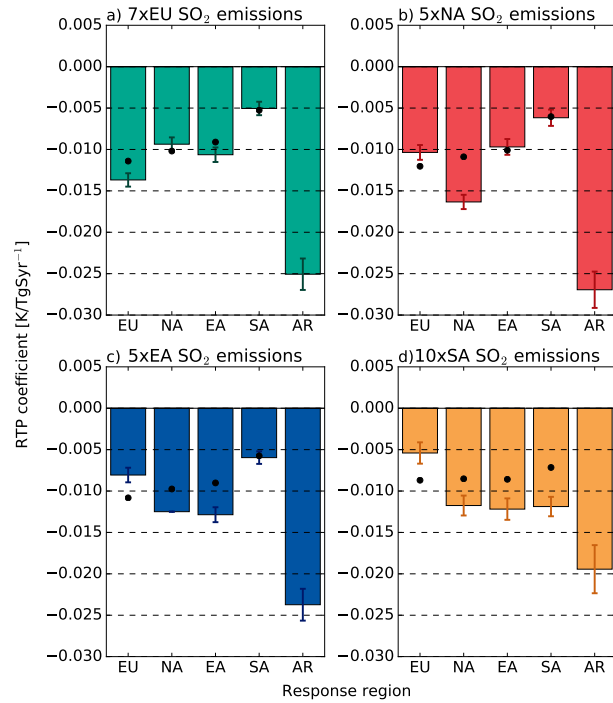


Figure 8. Regional RTP coefficients for SO₂ emission [K/TgSyr⁻¹] for a) EU emissions b) NA emissions c) EA emissions and d) SA emissions. Grey shading indicates that the temperature change is not statistically significant ($p > 0.05$) compared to the control simulation. The error bars show the standard error. Black dots indicate the zonal mean for the latitudes that cover each region.

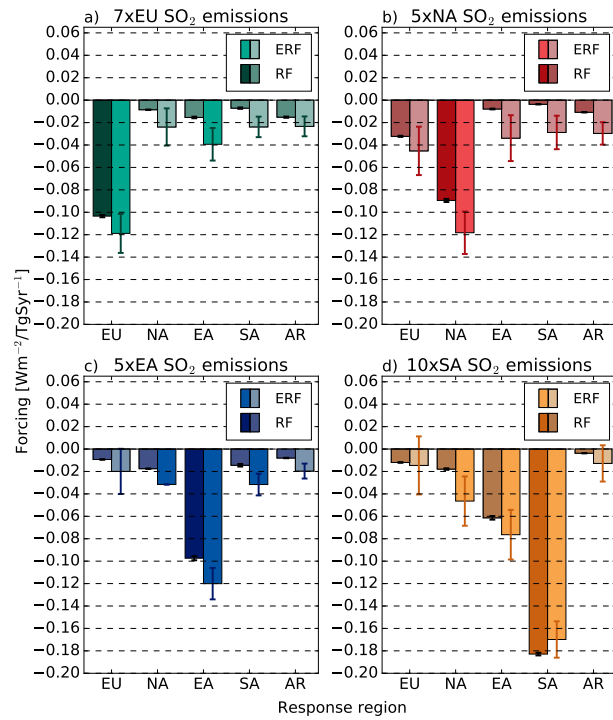


Figure 9. Regional RF and ERF for SO₂ emission [Wm⁻²/TgSyr⁻¹] for a) EU emissions b) NA emissions c) EA emissions and d) SA emissions. In each pair of bars the left bar indicated RF and the right bar indicated ERF. Grey shading indicates that the forcing response is not statistically significant ($p > 0.05$) compared to the control simulation. The error bars show the standard error.

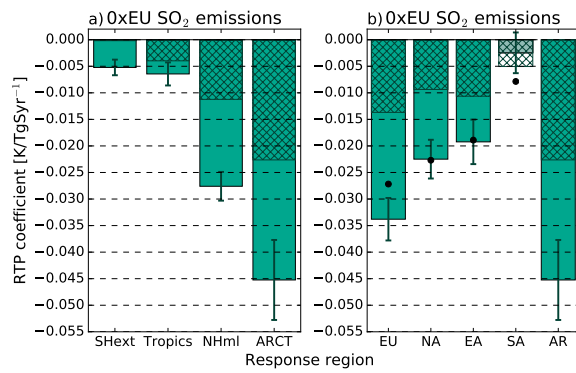


Figure 10. Latitudinal (a) and regional (b) RTP coefficients for 0xEU SO₂ emissions. [K/TgSyr⁻¹]. Grey shading indicates non-statistical differences ($p > 0.05$). The hatching indicated the RTP for 7xEU emissions (cf. Fig. 4 and 8) for easy comparison. The error bars show the standard error.

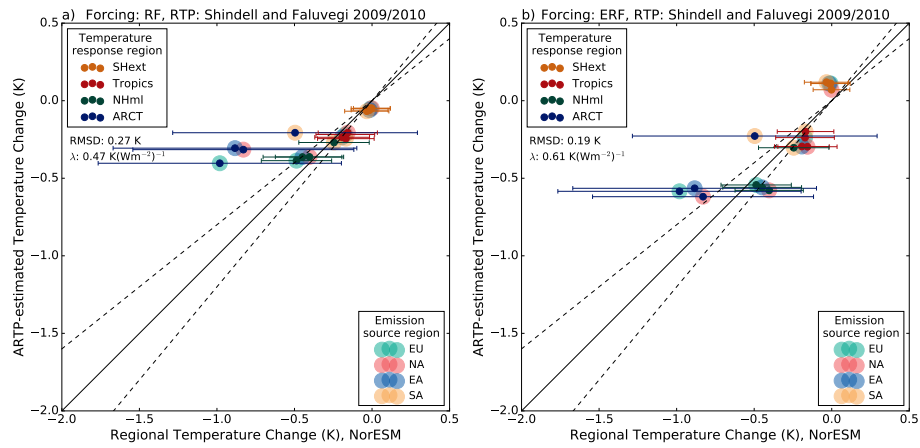


Figure 11. Regional temperature change from the coupled simulations (horizontal axis) compared with the estimated temperature response when using a) RF and b) ERF in combination with the RTP coefficients of Shindell and Faluvegi (2009), Eq. 1 with the climate sensitivity derived from the current experiments (vertical axis). The horizontal bars indicate one standard deviation for the temperature response in the coupled simulations. The dashed lines show $\pm 20\%$ agreement threshold.

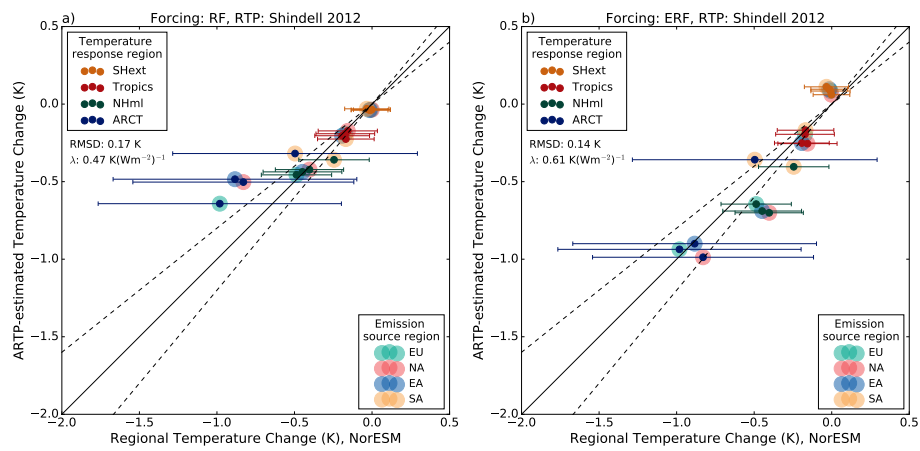


Figure 12. As Fig. 11 but with the RTP coefficients of Shindell (2012), Eq. 2 with the climate sensitivity derived from the current experiments.

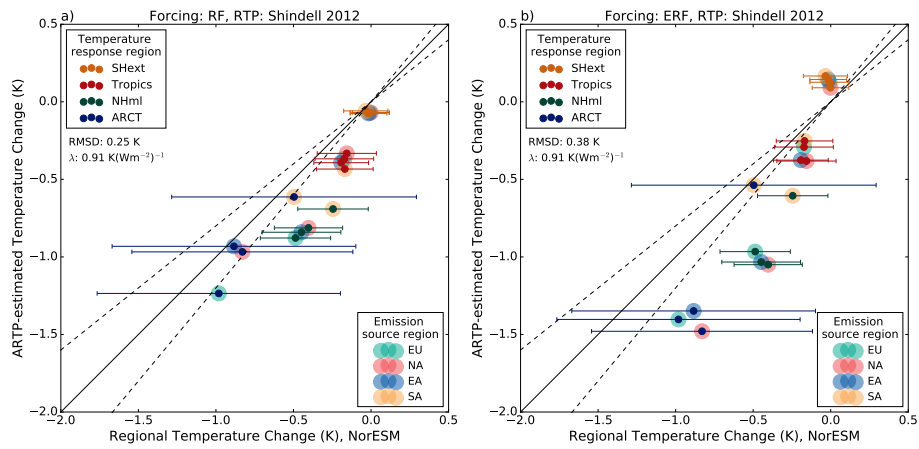


Figure 13. As Fig. 11 but with the RTP coefficients of Shindell (2012), Eq. 2 with the CO₂ sensitivity from Iversen et al. (2013).

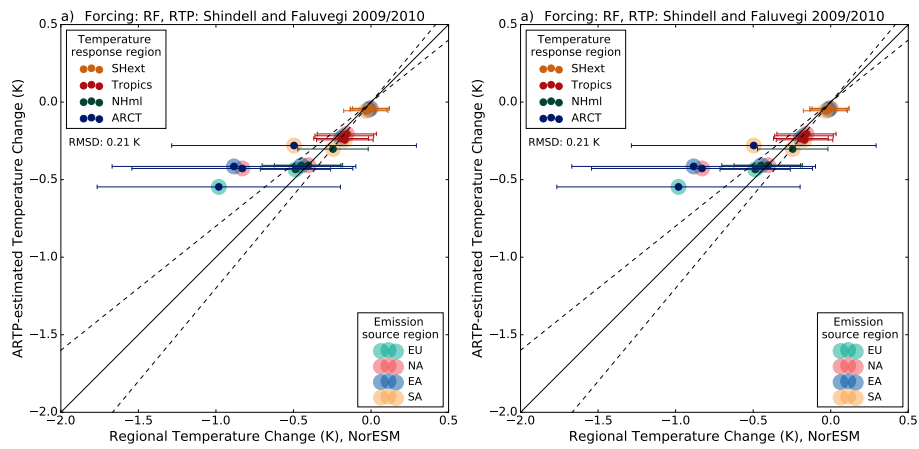


Figure 14. As Fig. 11 but with the RTP coefficients of Shindell and Faluvegi (2009), and with no climate sensitivity applied.